European Journal of Cardio-Thoracic Surgery 47 (2015) e34–e41
doi:10.1093/ejcts/ezu393 Advance Access publication 25 October 2014

ORIGINAL ARTICLE

Cite this article as: Meerang M, Boss A, Kenkel D, Broggini-Tenzer A, Bérard K, Lauk O *et al*. Evaluation of imaging techniques for the assessment of tumour progression in an orthotopic rat model of malignant pleural mesothelioma. Eur J Cardiothorac Surg 2015;47:e34–e41.

Evaluation of imaging techniques for the assessment of tumour progression in an orthotopic rat model of malignant pleural mesothelioma†

Mayura Meerang[a], Andreas Boss[b], David Kenkel[b], Angela Broggini-Tenzer[c], Karima Bérard[a], Olivia Lauk[a], Stephan Arni[a], Walter Weder[a] and Isabelle Opitz[a,*]

[a] Division of Thoracic Surgery, University Hospital Zurich, Zurich, Switzerland
[b] Department of Radiology, University Hospital Zurich, Zurich, Switzerland
[c] Laboratory for Molecular Radiobiology, University Hospital Zurich, Zurich, Switzerland

* Corresponding author. Division of Thoracic Surgery, University Hospital Zurich, Raemistrasse 100, 8091 Zurich, Switzerland. Tel: +41-44-2558802; fax: +41-44-2558805; e-mail: isabelle.schmitt-opitz@usz.ch (I. Opitz).

Received 20 June 2014; received in revised form 9 September 2014; accepted 10 September 2014

Abstract

OBJECTIVES: An orthotopic rat tumour recurrence model for malignant pleural mesothelioma (MPM) provides clinical similarity to patients and is useful for drug testing combined with surgical intervention. Importantly, a reliable imaging method is required allowing for noninvasive and repetitive evaluation of the tumour load. We compared the tumour load assessed by bioluminescence and magnetic resonance imaging (MRI) to the macroscopic tumour volume as a reference standard.

METHODS: A total of 500 000 syngeneic rat MPM cells transfected with luciferase were implanted underneath the parietal pleura of immunocompetent rats ($n = 13$). From the second day after implantation, bioluminescence measurements of the tumour load expressed as the maximum bioluminescent intensity (photon/second) were performed daily after intraperitoneal injection of the luciferase substrate, D-luciferin, to observe the first occurrence of tumour. Six days after the first detection of tumour, bioluminescence, MRI and macroscopic tumour volume measurement were conducted. For MRI, a 4.7-Tesla small animal imager equipped with a ^{1}H whole-body rat coil was employed using T_2-weighted fast spin-echo sequences. Tumour burden (mm^3) was quantified from magnetic resonance transverse images by two independent readers by manual segmentation. Finally, the tumour burden assessed by bioluminescence and MRI was correlated (Pearson's correlation) with the macroscopic measurement of tumour (ellipsoid) volume.

RESULTS: In all rats, a single tumour nodule was found at the inoculation site with a median macroscopic volume of 46 mm^3 (18–377 mm^3). For tumour burden quantification of MRIs, we observed good interobserver correlation ($R^2 = 0.81$, $P < 0.0001$) as well as significant association with the macroscopic tumour volume ($R^2 = 0.59$, $P = 0.002$). However, the signal intensity of bioluminescence did not correspond to the macroscopic tumour volume ($R^2 = 0.01$, $P = 0.76$).

CONCLUSIONS: MRI is a reliable and reproducible noninvasive *in vivo* imaging method for MPM tumour burden assessment for the present MPM model.

Keywords: Animal model • Rat • Mesothelioma • Magnetic resonance imaging • Bioluminescence

INTRODUCTION

Malignant pleural mesothelioma (MPM) is a rare and aggressive tumour. The major cause of MPM is attributed to the inhalation of asbestos fibres into the lung causing chronic inflammation and carcinogenesis. Although the use of asbestos in Europe was banned in the 1980s, the incidence is expected to rise in the next 5–10 years because of long disease latency [1]. Currently, the most widely used treatment approach includes a combination of chemotherapy (cisplatin plus pemetrexed [2]) plus macroscopic complete resection [3] with optional adjuvant radiotherapy [4]. Nonetheless, treatment response and long-term outcome are still very variable (reviewed in [5]). Therefore, it is important to explore novel targets as an alternative treatment option for MPM patients not responding to current protocols.

Besides chemotherapy directed against proliferative tumour cells, molecular targeted treatment and also immune therapy have drawn major interest [6, 7]. Prior to clinical trials, efficiency of new drug candidates have been tested *in vitro* using MPM primary

† Presented at the 22nd European Conference on General Thoracic Surgery, Copenhagen, Denmark, 15–18 June 2014.

cells or MPM human cell lines followed by preclinical animal models. However, *in vitro* conditions cannot fully mimic the tumour microenvironment that includes stromal cells, cytokines, chemokine, blood and oxygen gradient which all together play a major role in the growth, development and therapeutic resistance of MPM. Thus, a reliable *in vivo* model of MPM that closely resembles the clinical situation is required for testing the efficacy of new drug candidates.

Many studies have relied on the use of a subcutaneous or orthotopic xenograft immunodeficient tumour model to test the efficacy of a new compound as well as its pharmacokinetics and toxicities *in vivo* [8–11]. However, the immune system plays an important role in tumour biology and may influence the regression of an MPM [12, 13]. Thus, an immunodeficient animal model cannot entirely represent the clinical situation.

Our group has established an orthotopic immunocompetent rat model by implanting syngeneic rat mesothelioma cells (IL45) underneath the parietal pleura, which regrows after surgical resection [14, 15]. This model was employed to test the efficacy of a multimodal treatment model combining surgery with intrapleural cisplatin treatment or immunochemotherapy [15, 16]. However, an *in vivo*, noninvasive imaging method is needed for reliable detection and quantification of the tumour burden. Fluorescence, bioluminescence (Bli), computed tomography (CT) and magnetic resonance (MR) have been employed for orthotopic MPM tumour imaging [10, 11]. We created Bli-expressing clones of an IL45 cell line (IL45-Luc) by stable transfection [17]. The implantation of the IL45-Luc cells in an immune-competent rat generated tumour masses that could be detected by the Bli imager as soon as 3 days after inoculation. The IL45-Luc-derived tumour displayed the same histology as tumours derived from un-transfected IL45 cells [17].

Discordance between Bli and the macroscopic tumour volume measured was observed in some cases; therefore, we implemented an MR imaging protocol in a small animal imager as a third independent technique to assess the tumour burden. Here, we present an approach to quantify tumour burden from MR images. We investigated the correlation between the tumour burden quantified from MR images and Bli signal with the tumour volume measured macroscopically as a reference standard.

MATERIALS AND METHODS

Tumour inoculation

The IL45-Luc cell line was maintained as previously described [17]. Immunocompetent male Fischer 344 rats ($n = 13$) (F344/NCrHsd; 200–250 g) were purchased from Harlan Laboratories (the Netherland) and housed according to standard guidelines of the Swiss animal health-care law. Experiments were approved by the veterinary office of Zürich. We inoculated 500 000 IL45-Luc cells suspended in 50 µl of Dulbecco's phosphate-buffered saline underneath parietal pleura as previously described [17]. For analgesia, all rats received paracetamol (30 mg/kg) 30 min before and 4 h after surgery.

Bli measurement began two days after inoculation, and continued daily until Bli signal appeared ($n = 13$). The first Bli signals were detected between 2 and 6 days after inoculation. After the first detection, tumours were grown for 6 days in order to avoid >15% body weight loss. Seven rats received daily treatment of a hedgehog antagonist which inhibits tumour cell proliferation by 10%, generating variation in tumour volume. Bli and MR imaging were conducted prior to euthanization and the macroscopic tumour volume measurement.

Bioluminescence imaging and the analysis

Animal preparation for Bli imaging was performed as previously described [17]. Bli images were sequentially acquired with exposure time of 60 s until the highest Bli signal was detected. We used IVIS 200 living image software (Caliper Life Sciences, Inc., MA, USA) to construct pseudo colour images of Bli signal overlaid on the animal's whole-body picture. A region of Bli [region of interest (ROI)] was selected and quantified for area (mm^2) and total Bli signal (photon/second). Total Bli emission was plotted against time after D-luciferin injection. The peak of Bli signal was taken for analysis.

Magnetic resonance imaging and the quantification of tumour volume

Magnetic resonance imaging (MRI) was performed with a Bruker 4.7 T Pharmascan 47/16 US with a gradient strength of 375 mT/m and a slew rate of 3375 T/ms. A linear polarized whole-body mouse ^1H radiofrequency coil was applied for spin excitation and signal reception. During the scan, the rats were anaesthetized with isoflurane (Attane; Minrad I, Buffalo, NY, USA). On-line respiration monitoring was performed with an MR-compatible physiology unit (SA Instruments, Inc., NY, USA). After gradient-echo localizers in three spatial directions, the imaging protocol consisted of a 2D encoded T_2-weighted fast spin-echo sequence (TR/TE, 3528 ms/11 ms; effective TE, 45 ms; echo train length, 8; matrix, 384 × 384; field of view, 60 × 60 mm^2; slice thickness, 1 mm; number of acquisitions, 5; interslice gap, 0.5 mm) in transverse, sagittal and coronal orientation. After data acquisition, data sets were transferred to an off-line computer.

Two observers quantified tumour volume independently. Image J software (Wayne Rasband, National Institutes of Health, MD, USA) was used to define the tumour area on the T_2-weighted data set in transverse orientation by free hand drawing for each slice depicting tumour tissue. Sagittal and coronal data sets were opened in parallel to assist for tumour area identification. Criteria for tumour identification were intermediate hyperintense signal on T_2-weighted imaging (hypointense to pleural effusion, hyperintense to the anatomical thoracic wall, nodular masses, pleural masses, whereas non-mass-like hyperintensity of the thoracic wall was regarded as postinterventional changes caused by thoracotomy). In case tumour and scar tissues were indistinguishable, the margin of the tumour was defined at the middle of the rib. The histological examination showed that the tumour never invaded tissues behind the middle margin of the ribs. The tumour value for each space between two image slices was calculated by the formula

$$\text{Volume} = \frac{(\text{Area}_1 + \text{Area}_2) * 1.5 \text{ mm slice thickness}}{2},$$

the complete tumour volume being obtained by integrating the volumes of all slice intervals (see Fig. 1).

EXPERIMENTAL

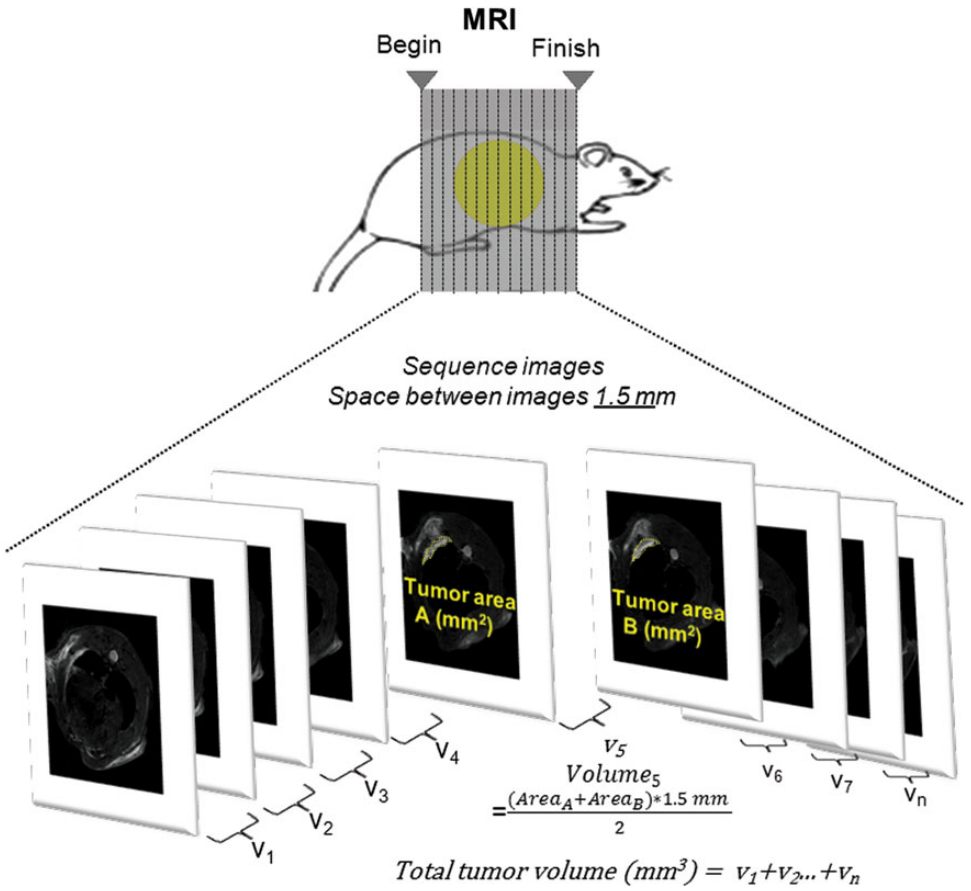

Figure 1: Diagram showing tumour volume quantification from MR images.

Macroscopic tumour volume quantification

After euthanasia with an overdose of pentobarbital and exsanguination, we excised the chest wall that contained the tumour nodule. The length (*a*) and width (*b*) of the tumour were measured with a slide callipers. The tumour area (mm^2) was calculated by the ellipsoid formula: area = $\pi \times a/2 \times b/2$. The thoracic wall was cut at the thickest part and fixed in formalin for histological analysis. The thickness of tumour (*c*) was measured on the H&E section. Finally, the tumour volume was approximated using the ellipsoid formula: $V = 4/3\ \pi \times a/2 \times b/2 \times c/2$ [15].

Histology and proliferation index

Tissues were fixed in 4% formalin for 24 h and then de-calcified in EDTA solution for 2–3 weeks. Afterwards, they were intensively washed in water, dehydrated in a series of alcohol solutions and embedded in paraffin. Tissues were cut at 3 μm thickness and stained for H&E and collagen using the Sirius red method. The proliferation index with Ki67 (rabbit anti-Ki-67, CMC27531021; Cell Marque) was quantified as the percentage of positive Ki67 tumour nuclei per total tumour nuclei [18].

Statistical analysis

Statistical analysis has been performed by computation of Pearson's correlation coefficient using Prism 5 (GraphPad software, Inc., CA, USA). A *P* value of less than 0.05 was considered significant. The intraclass correlation coefficient was computed by SPSS 22.

RESULTS

Characteristics of IL45-Luc-derived tumour

At autopsy (6 days after the first tumour detection), a single tumour nodule was visible at the injection site (Fig. 2A) in all rats with a median macroscopic tumour volume of 46 mm^3 (range; 18–377 mm^3, Supplementary Table 1). As described previously, tumours derived from IL45-luc were of the sarcomatoid mesothelioma subtype (Fig. 2B). The stromal compartment including fibroblasts, immune cells, extracellular matrix and vessels was present (Fig. 2B and C). Tumours were highly proliferative as shown by the over 70% Ki-67 staining index (Fig. 2D), and the tumours were without any necrotic area.

Bioluminescence imaging

The median maximum Bli signal was observed at 21.5 min (range; 16–32 min) after injection of D-luciferin with the median bioluminescent value of 1.21×10^7 p/s (range; 3.6×10^6–4.9×10^7 p/s, Supplementary Table 1). We observed postoperative inflammation localized at the thoracotomy site in some rats and reduced bioluminescence signal within this area (data not shown). Tumour areas (2D) quantified from Bli were 30 times (range; 12–45 times)

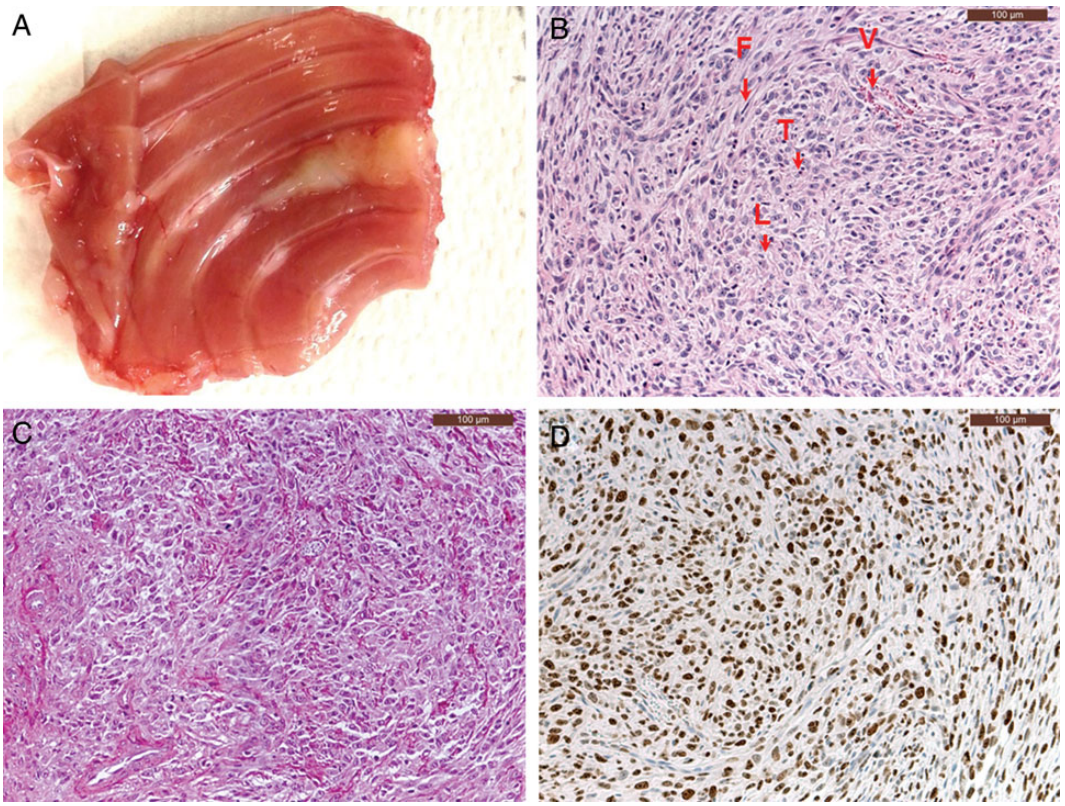

Figure 2: (**A**) Macroscopic appearance of a tumour derived from IL45-Luc cells. A white tumour nodule is found around the injection site. (**B**) In an H&E staining and indicated by arrow; tumour cells (T), stromal part containing blood vessels (V), lymphocytes (L) and fibroblasts (F). (**C**) Collagen staining showing the presence of collagen bundles (red) infiltrates. (**D**) Ki67 staining (brown) of tumour cells.

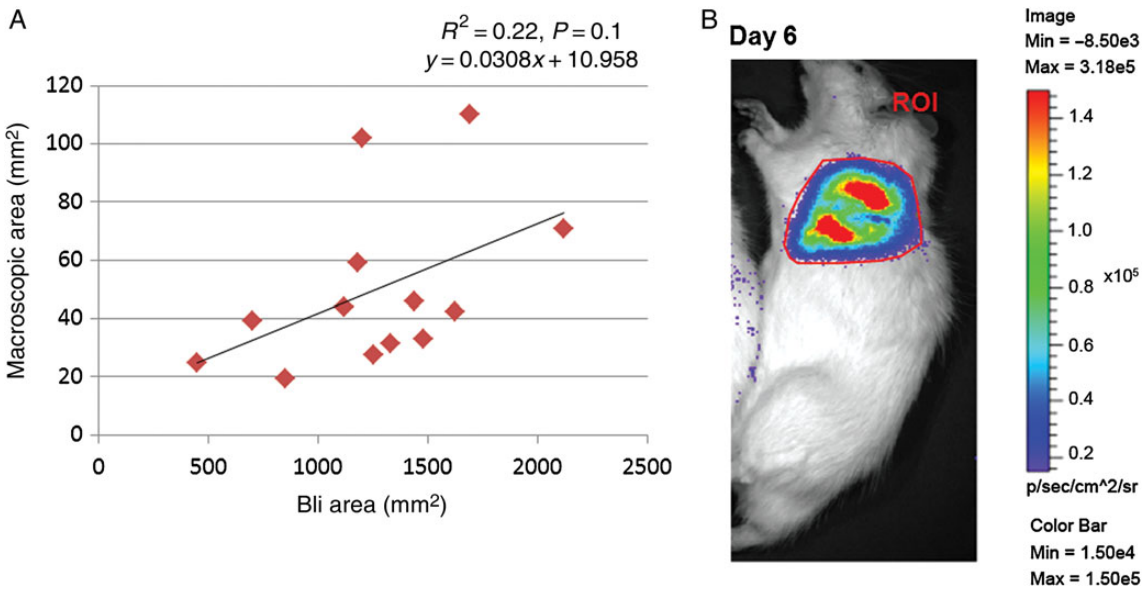

Figure 3: (**A**) A trend of positive correlation between tumour area quantified in Bli images and macroscopically ($n = 13$). (**B**) Example of Bli image of a rat (ROI: region of interest).

larger than the actual macroscopic tumour area but showed a trend of positive correlation ($R^2 = 0.22$, $P = 0.1$) (Fig. 3A). However, the total tumour burden quantified from the Bli image (photon/second) did not correlate with macroscopic tumour volume (Fig. 6B).

Magnetic resonance images

Tumour nodules appeared within 5–14 image sections, showing irregular shape. Tumour and postoperative scar were visible as slightly hyperintense signals compared with the chest wall,

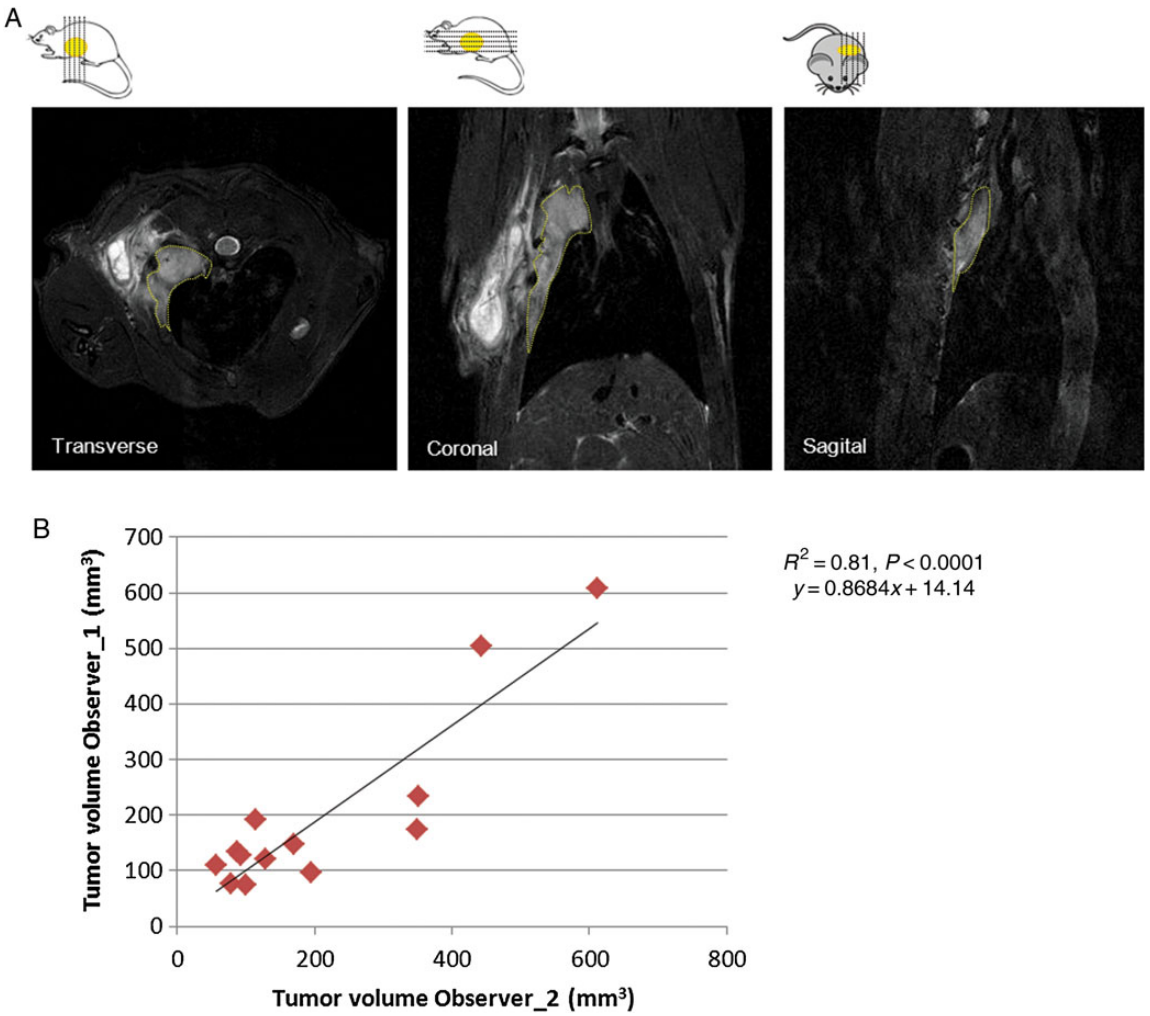

Figure 4: (**A**) Example of MR images (transverse/coronal/sagittal); the margins of tumour area are indicated with yellow lines. (**B**) Significant correlation of tumour volumes quantified in transverse images by two independent observers ($n = 13$).

whereas strong hyperintensity represents areas of inflammation or fluid collections (Fig. 4A). The correlation of tumour volume measured from MR images by the two observers was highly significant with a Pearson correlation coefficient of 0.81 (Fig. 4B) and intraclass correlation coefficient of 0.903. For the further analyses, the average of tumour volumes quantified by the two observers was used. The median tumour burden quantified from MR images was 145.4 mm^3 (range; 77.7–609.8 mm^3, Supplementary Table 1) and was 3.5 (median) times higher than the one measured macroscopically (range; 0.7–7.6 times). We could not observe any correlation between tumour burden quantified from MR images and total Bli signal (Fig. 5A and B). However, tumour volume measured macroscopically and from MRI images correlated significantly (Fig. 6A).

Discussion

Our orthotopic immune-competent rat MPM model provides a tumour microenvironment that closely reflects the clinical situation. It was proved useful for testing new drug candidates as well as surgical intervention and will provide greater benefit if the tumour can be monitored repetitively and noninvasively. MR imaging and Bli were assessed for their reliability in tumour burden quantification by comparing with the macroscopic tumour volume. In this study, we found that MR imaging provides more reliable tumour burden assessment than Bli as it correlates strongly with the macroscopic tumour volume. Quantification of tumour burden from MR images is a reliable approach as the measurements can be reproduced independently by two observers. MR imaging has been successfully applied for the visualization of MPM in the orthotopic mouse model of MPM as well as other models of solid tumours [10, 19].

The quantification of tumour volume from MR images was feasible and reproducible (good interobserver agreement). Nevertheless, we observed that fibrous postoperative scar interferes with the quantification of tumour volume from MR images. A possible solution for the discrimination between tumour and the postoperative changes including inflammation and fibrosis might be the use of 'diffusion-weighted imaging' (DWI). 'Apparent diffusion coefficient' values, which are commonly used to quantify the results of DWI, are described as the specific parameter for the differentiation of recurrence of tumour and scar in breast cancer [20]. However, the role of DWI in the differentiation of mesothelioma from postoperative changes is hitherto unknown. Furthermore, an impeded diffusion that is seen in tumours can also be seen in inflammatory or infected areas due to the increased cellular density in those areas [21]. Therefore, DWI might be an interesting tool for the differentiation of tumours and postoperative changes in the future, but the potential

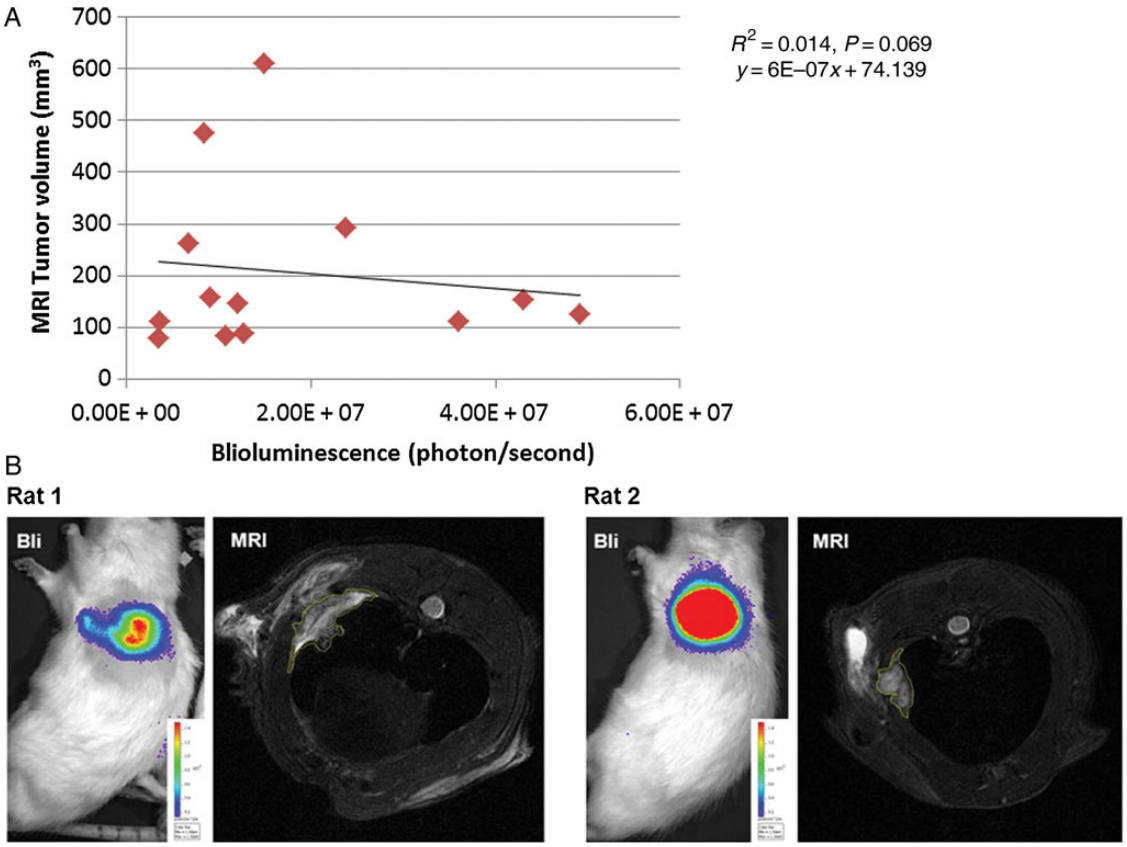

Figure 5: (**A**) Scatter plot between tumour volume quantified from MR images and Bli signal showing no correlation ($n = 13$). (**B**) Images showing typical discrepancies between tumour volume visualized by MR and Bli signal. Rat 2 shows strong Bli signal (red); however, the tumour size visible by MRI is smaller than that of Rat 1, which exhibited lower Bli intensity.

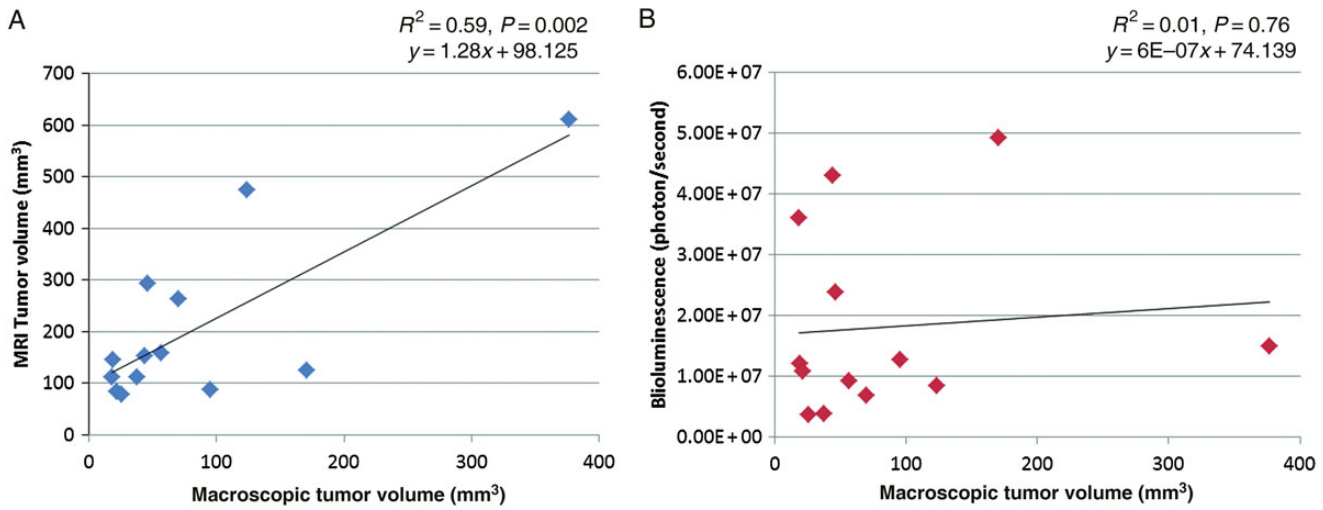

Figure 6: Correlation between macroscopic tumour volume versus MRI and Bli: (**A**) Positive correlation between tumour volume quantified from MR images (mm^3) (average of two observers) and macroscopic tumour volume. (**B**) Bli signal (photon/second) does not correlate with macroscopic tumour volume.

application for mesothelioma needs to be evaluated. Furthermore, a semi-automated approach has been successfully applied for the measurement of MPM tumour thickness in CT scan images [22]. A computer interface requires users to indicate an initial end-point; thereafter, it determines the corresponding terminal end-point automatically using a greyscale threshold. It showed high agreement with manual quantification and thus may also be applicable for tumour volume quantification from MR images that we acquired.

The tumour volume obtained from MR images was about two times bigger than the volume quantified macroscopically. This systemic positive bias could be explained by continuous underestimation of tumour thickness measured from H&E sections due to shrinkage of tissues after a fixation and dehydration procedure. Indeed the thickness of the tumour measured from MR images was larger than the thickness measured from H&E sections (data not shown).

Several studies in subcutaneous or intraperitoneal tumour models showed strong correlation between Bli and actual tumour volume [23, 24]. In our study, 2D analyses (tumour area) of both Bli and macroscopic observation show only a trend of positive correlation; this may be explained by the small sample size. However, tumour areas visualized in Bli images were overestimated probably due to the inclusion of light radiance. Total bioluminescent emission (3D) correlates with neither the macroscopic tumour volume nor MRI tumour burden. This discordance between Bli and tumour volume can be explained by several reasons. The emission of Bli signal depends on the extent of luciferase expression and the penetration depth of light [25]. In our model, tumour nodules were deeply embedded in the thoracic cavity. In some cases, Bli can be hindered near the operation site by tissue thickening that results from inflammation and postoperative scar. Accurate injection of D-luciferin into the intraperitoneal cavity is crucial as, in some cases, no Bli signal was detected after injection. Upon re-injection of D-luciferin into the same rat, Bli signal appeared immediately. Intravenous administration may be a better method for applying the correct dosage of D-luciferin; however, it is practically difficult to inject sequentially large volumes of substrate intravenously in rats (authors' own experience). There are different types of information obtained from Bli signal versus total tumour volume. Bli signal can only be emitted from living tumour cells and therefore indicates the burden of tumour cells alone, excluding apoptotic and necrotic cells. It is a sensitive detection method and is suitable for early detection of tumour growth after testing a compound that causes necrosis and apoptosis. However, Bli signal does not include the stromal fraction. Total tumour volume can be represented by MR images and macroscopic observations. Thus, the combination of the two methods may provide an advantage and distinguish the effect of drugs on the stromal compartment.

Disadvantages of the MR examination are that they are relatively costly examinations due to the purchasing costs and the maintenance of the MR imager. The duration of MR image acquisition varied from 45 min to 1 h per rat, hence increasing anaesthesia and experimental duration. In principle, metals could be a problem, e.g. implanted material after surgery, due to the propensity of these materials to cause distortions of the magnetic field. However, the material used in this study did not cause relevant image artefacts. On the other hand, Bli provides a faster imaging method as two rats can be placed in the Bli imaging chamber and measured simultaneously for a maximum of 35 min. However, a big volume of D-luciferin is required for a rat weighting between 250 and 300 g and the injection caused stress especially in repetitive measurements.

In our specific orthotopic rat MPM model, MR imaging provided more reliable tumour burden quantification. However, the measurements in rats were hindered by the postoperative scar and inflammation, which are common problems that impede tumour mass detection in humans. This model will be further defined to better discriminate between tumour and postoperative scar. In our study, a small thoracotomy was performed for tumour inoculation and we observed that the scar tissue and inflammation was diminishing over the recovery time of 6 days. By inoculating fewer tumour cells, the duration of the experiment may be extended to allow healing and recovery from inflammation before the assessment. These imaging techniques may be applied for tumour load assessment following major surgery such as radical pleurectomy and extrapleural pneumonectomy; however, proper recovery time needs to be validated. Moreover, contrast medium for MR imaging will be tested for its potential application to discriminate tumour from scar. Advances in the development of imaging methods for such orthotopic preclinical animal models will represent great progress in the field of cancer research for therapeutic development.

SUPPLEMENTARY MATERIAL

Supplementary material is available at *EJCTS* online.

ACKNOWLEDGEMENTS

We thank Martin Pruschy for providing the Bli imager and support with the preliminary assessment. In addition, we thank Rolf Stahel and Emanuela Felley-Bosco for providing helpful and insightful comments for the project. P. Vogt is acknowledged for providing assistance for interpretation of tumour histology. We are also indebted to Chloé Spichiger for her editorial assistance in the preparation of the manuscript.

Funding

This work was supported by a Swiss National Science Foundation professorship to Isabelle Opitz.

Conflict of interest: none declared.

REFERENCES

[1] Robinson BW, Musk AW, Lake RA. Malignant mesothelioma. Lancet 2005; 366:397–408.
[2] Vogelzang NJ, Rusthoven JJ, Symanowski J, Denham C, Kaukel E, Ruffie P *et al.* Phase III study of pemetrexed in combination with cisplatin versus cisplatin alone in patients with malignant pleural mesothelioma. J Clin Oncol 2003;21:2636–44.
[3] Rusch V, Baldini EH, Bueno R, De Perrot M, Flores R, Hasegawa S *et al.* The role of surgical cytoreduction in the treatment of malignant pleural mesothelioma: meeting summary of the International Mesothelioma Interest Group Congress, September 11–14, 2012, Boston, Mass. J Thorac Cardiovasc Surg 2013;145:909–10.
[4] Rusch V, Rosenzweig K, Venkatraman E, Leon L, Raben A, Harrison L *et al.* A phase II trial of surgical resection and adjuvant high-dose hemithoracic radiation for malignant pleural mesothelioma. J Thorac Cardiovasc Surg 2001;122:788–95.
[5] Opitz I. Management of malignant pleural mesothelioma-The European experience. J Thorac Dis 2014;6:S238–S52.
[6] Calabro L, Maio M. Immune checkpoint blockade in malignant mesothelioma: a novel therapeutic strategy against a deadly disease? Oncoimmunology 2014;3:e27482.
[7] Belli C, Fennell D, Giovannini M, Gaudino G, Mutti L. Malignant pleural mesothelioma: current treatments and emerging drugs. Expert Opin Emerg Drugs 2009;14:423–37.
[8] Shi Y, Moura U, Opitz I, Soltermann A, Rehrauer H, Thies S *et al.* Role of Hedgehog signaling in malignant pleural mesothelioma. Clin Cancer Res 2012; 18:4646–56.
[9] Li H, Lui N, Cheng T, Tseng HH, Yue D, Giroux-Leprieur E *et al.* Gli as a novel therapeutic target in malignant pleural mesothelioma. PLoS One 2013;8:e57346.
[10] Nayak TK, Bernardo M, Milenic DE, Choyke PL, Brechbiel MW. Orthotopic pleural mesothelioma in mice: SPECT/CT and MR imaging with HER1- and HER2-targeted radiolabeled antibodies. Radiology 2013;267:173–82.
[11] Saito Y, Furukawa T, Arano Y, Fujibayashi Y, Saga T. Comparison of semi-quantitative fluorescence imaging and PET tracer uptake in mesothelioma models as a monitoring system for growth and therapeutic effects. Nucl Med Biol 2008;35:851–60.

[12] Robinson BW, Robinson C, Lake RA. Localised spontaneous regression in mesothelioma—possible immunological mechanism. Lung Cancer 2001; 32:197–201.
[13] Scherpereel A, Grigoriu BD, Noppen M, Gey T, Chahine B, Baldacci S *et al*. Defect in recruiting effector memory CD8+ T-cells in malignant pleural effusions compared to normal pleural fluid. BMC Cancer 2013;13: 324.
[14] Lardinois D, Jung FJ, Opitz I, Rentsch K, Latkoczy C, Vuong V *et al*. Intrapleural topical application of cisplatin with the surgical carrier Vivostat increases the local drug concentration in an immune-competent rat model with malignant pleuromesothelioma. J Thorac Cardiovasc Surg 2006;131:697–703.
[15] Opitz I, Lardinois D, Arni S, Hillinger S, Vogt P, Odermatt B *et al*. Local recurrence model of malignant pleural mesothelioma for investigation of intrapleural treatment. Eur J Cardiothorac Surg 2007;31:773–8.
[16] Ampollini L, Soltermann A, Felley-Bosco E, Lardinois D, Arni S, Speck RF *et al*. Immuno-chemotherapy reduces recurrence of malignant pleural mesothelioma: an experimental setting. Eur J Cardiothorac Surg 2009;35: 457–62.
[17] Shi Y, Hollenstein A, Felley-Bosco E, Fraefel C, Ackermann M, Soltermann A *et al*. Bioluminescence imaging for in vivo monitoring of local recurrence mesothelioma model. Lung Cancer 2011;71:370–1.
[18] Bitanihirwe BK, Meerang M, Friess M, Soltermann A, Frischknecht L, Thies S *et al*. PI3K/mTOR signaling in mesothelioma patients treated with induction chemotherapy followed by extrapleural pneumonectomy. J Thorac Oncol 2014;9:239–47.
[19] Montelius M, Ljungberg M, Horn M, Forssell-Aronsson E. Tumour size measurement in a mouse model using high resolution MRI. BMC Med Imaging 2012;12:12.
[20] Rinaldi P, Giuliani M, Belli P, Costantini M, Romani M, Distefano D *et al*. DWI in breast MRI: role of ADC value to determine diagnosis between recurrent tumor and surgical scar in operated patients. Eur J Radiol 2010;75: e114–e23.
[21] Kwee TC, Takahara T, Ochiai R, Koh D-M, Ohno Y, Nakanishi K *et al*. Complementary roles of whole-body diffusion-weighted MRI and 18F-FDG PET: the state of the art and potential applications. J Nucl Med 2010;51:1549–58.
[22] Armato SG III, Ogarek JL, Starkey A, Vogelzang NJ, Kindler HL, Kocherginsky M *et al*. Variability in mesothelioma tumor response classification. AJR Am J Roentgenol 2006;186:1000–6.
[23] Feng M, Zhang J, Anver M, Hassan R, Ho M. In vivo imaging of human malignant mesothelioma grown orthotopically in the peritoneal cavity of nude mice. J Cancer 2011;2:123–31.
[24] Choy G, O'Connor S, Diehn FE, Costouros N, Alexander HR, Choyke P *et al*. Comparison of noninvasive fluorescent and bioluminescent small animal optical imaging. BioTechniques 2003;35:1022–6. 8–30.
[25] Badr CE, Tannous BA. Bioluminescence imaging: progress and applications. Trends Biotechnol 2011;29:624–33.